J. Fluid Mech. (1985), *vol.* 152, *pp.* 49–66
Printed in Great Britain

Observation and analysis of the Mach reflection of weak uniform plane shock waves. Part 1. Observations

By J. M. DEWEY AND D. J. McMILLIN
University of Victoria, Victoria, B.C., Canada V8W 2Y2

(Received 7 February 1984)

Shock fronts and fluid-particle trajectories throughout a two-dimensional shock wave flow have been measured by multiple schlieren photography in a detailed study of the Mach reflection from a 10° wedge of plane uniform shocks with Mach numbers of 1.105, 1.240 and 1.415. Correction of optical distortions throughout the field of view permitted the positions and shapes of the shock fronts and the magnitudes and directions of the particle velocities to be measured with a high degree of accuracy. No departure from self-similarity of the flow fields could be detected. The cross-sections of the reflected shocks were found to be circular and centred on a point which moved with the velocity of the flow behind the incident shock. The triple-point trajectories were linear. The velocity of the curved Mach stem shock was found to be constant at any one height above the wedge surface and to decrease monotonically with height. A deviation from perpendicularity was noticed where the Mach stems met the surface of the wedge, the shocks having a slight forward inclination of as much as 1°. The experimental results cannot be completely explained using the classical three-shock theory and an alternative model for weak Mach reflection is developed in Part 2 of this paper.

1. Introduction

Many optical techniques have been applied to the study of shock waves. The most widely used are shadow and schlieren photography, which date back to the early work of Mach (1878) and Boys (1893). These two techniques, which are very similar to each other, provide an accurate record of the positions of shock fronts and other large density gradients such as may occur across contact surfaces between different gases. From a high-speed sequence of shadow or schlieren photographs shock velocities may be determined and changes in the physical properties of the gas across the shocks computed. However, little or no information is provided about the gas flow elsewhere, in regions where the density gradients are not large.

The flow-fields associated with shock waves can be visualized using an interferometer, and an analysis of interferograms can map the density throughout the observed field (Ben-Dor & Glass 1979; Dewey *et al.* 1983). However, for unsteady shock waves it is not possible to derive from the density any of the other physical properties of the gas, which is left in a state of spatially varying entropy.

In an attempt to overcome some of the limitations of shadow, schlieren and interferometric photography, a fourth technique has been developed in which flow tracers are introduced into the gas immediately before the arrival of the shock wave. This technique has been applied to the study of spherical, cylindrically symmetric, and one- and two-dimensional plane shock flows (Dewey 1964, 1971; Dewey, McMillin

& Classen 1977; Dewey & McMillin 1981; Dewey & Whitten 1975; Dewey & Walker 1975). It has been shown (Dewey 1964, 1971) that a measurement of the time-resolved trajectories of the gas particles within a shock wave permits a calculation of all the other physical properties of the flow, namely the particle velocity, density and hydrostatic pressure, from which, in turn, the dynamic pressure, temperature and specific energy can be determined. This technique has been refined and used in a study of the Mach reflection of plane uniform shock waves, and the results are presented here.

Extensive reviews of the phenomenon known as Mach reflection have been given by Ben-Dor & Glass (1978, 1979, 1980), Henderson & Lozzi (1979) and Henderson & Siegenthaler (1980), and, insofar as they are relevant to the present study, the results of these and other workers will be discussed in Part 2 of this paper (Dewey & McMillin 1985). It is sufficient to say at this point that the method which has been found convenient for describing the Mach reflection of a plane shock at a plane surface is based on the assumptions that the flow is self-similar, and that non-stationary shock flows such as those produced in a shock tube can be made pseudo-stationary by the superposition of appropriate flow velocity vectors (Jones, Martin & Thornhill 1951). A pseudo-stationary flow is considered to pass through and be deflected by stationary incident, reflected and Mach stem shocks, and the flow may be analysed using oblique shock theory. Evaluation of the pseudo-stationary assumption is not possible unless the particle trajectories within the flow are known experimentally. From schlieren photographs alone the direction of the flow at the triple point can be determined from an observation of the contact or slip surface separating the gas which has traversed the incident and reflected shocks from the gas which traversed the Mach shock (Henderson & Siegenthaler 1980). In the present study the magnitude and direction of the particle flow is measured throughout the field of view, thus accommodating an evaluation of the assumptions made in the application of oblique shock theory.

The particle trajectory technique has been used to observe the Mach reflection from a 10° wedge of plane uniform shocks with Mach numbers of 1.105, 1.240 and 1.415. The 10° wedge angle was chosen to maximize the length of the Mach stem and thus permit the measurement of the maximum number of particle trajectories in the region behind the Mach stem. A larger wedge angle would have produced a smaller Mach stem region, and a smaller angle, while producing only a small increase in the size of the Mach stem, would have produced a weaker reflected shock.

2. Experimental procedures

2.1. *The optical system*

The optical system used to observe the particle trajectories produced by the shock reflections was essentially that described by Dewey & Walker (1975). A schematic drawing of the system is shown in figure 1. One of the windows in the working section of a 76×254 mm cross-section rectangular shock tube was replaced by a 300×254 mm rectangular front-surface stainless-steel plane mirror polished to schlieren quality. 721 holes, each 0.33 mm in diameter, were drilled through the mirror on a rectangular grid at a spacing of 10 mm. Behind the mirror was a chamber filled with a filtered smoke produced by mixing the vapours of concentrated hydrochloric acid and ammonium hydroxide solutions. Shortly before the arrival of a shock wave a pressure of approximately 100 mm of mercury was applied to the smoke chamber, which caused coherent laminar jets of smoke to be injected into the shock tube through the holes in the mirror. The pressure applied to the smoke

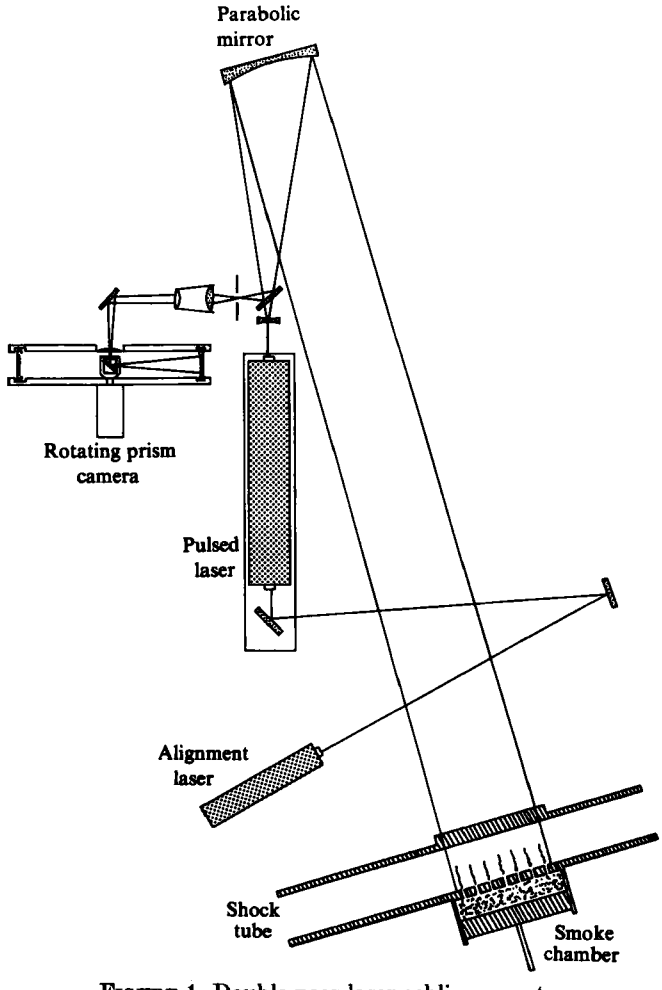

FIGURE 1. Double pass laser schlieren system.

chamber was carefully chosen so that the jets remained laminar as they traversed the 76 mm width of the tube. The pressure was applied at a time such that the jets had almost reached the window on the other side of the shock tube when the shock front first arrived in the field of view. The laminar jets were viewed end-on by a schlieren system and appeared as a grid of individual particle tracers, as shown in figure 2.

The light source for the schlieren system was a ruby laser, Q-switched by a transverse Pockels cell. The duration of each pulse was approximately 50 ns. Because consistent results could not be obtained at the intended pulsing frequency of 40 kHz, series of four experiments were carried out under identical conditions. The laser was pulsed at 10 kHz in each experiment with the pulse trains triggered so that, when the four sets of results were combined, an almost uniform spacing between photographs was obtained at an effective frequency of 40 kHz. Uniform spacing in the combined set of photographs was not assumed, however. The time of each pulse in each experiment was recorded relative to the arrival of the shock front at the leading edge of the wedge.

Light from the laser passed through a diverging lens to produce a virtual point

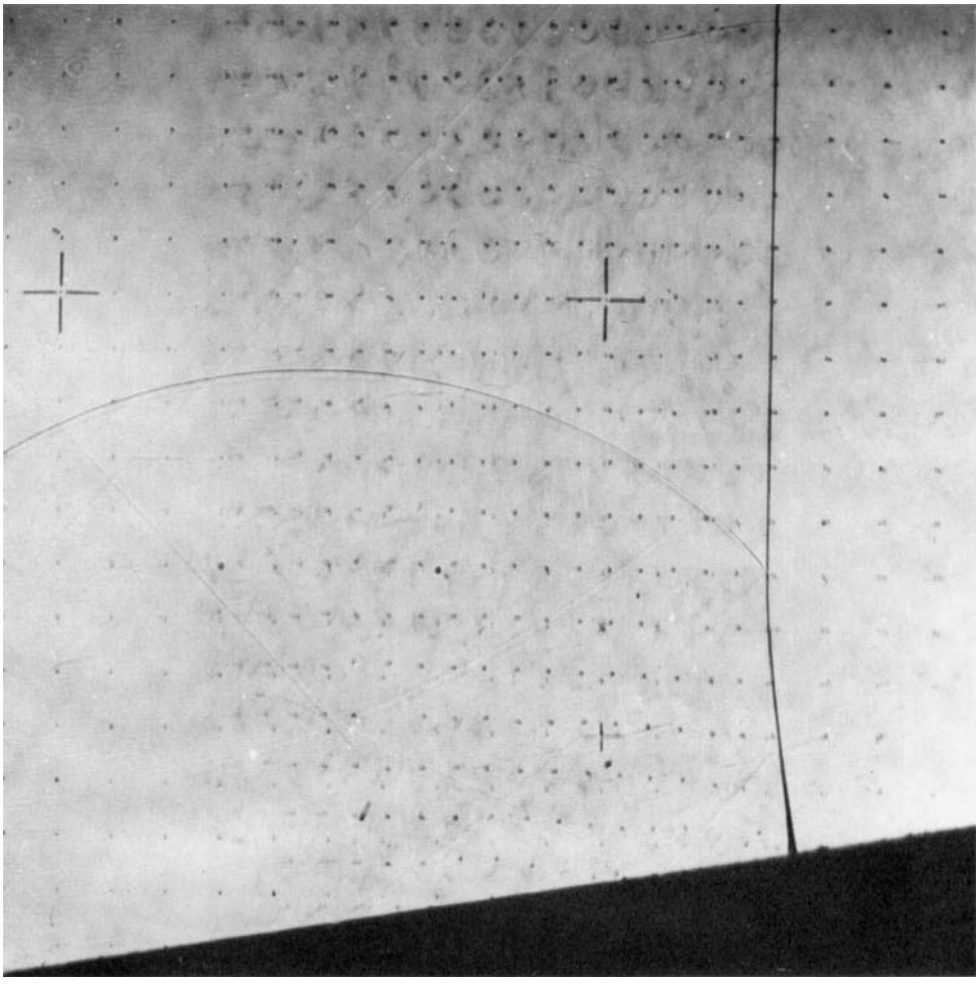

FIGURE 2. Schlieren photograph of shock fronts and particle tracers in experimental series 3. The thickening of the schlieren image of the foot of the Mach stem was apparent in all photographs in all experimental series. No explanation is offered for this boundary effect. Several transverse shocks can be seen. These occur because the diaphragm rupture is not a one-dimensional event. These shocks are extremely weak, and do not affect the experimental results in any measurable way.

source at the principal focus of a parabolic mirror of 300 mm diameter and 1.5 m focal length. The resulting parallel beam passed through the window section and was normally reflected from the front-surface plane mirror. The returning beam was deflected by a beam splitter through a lens system into a rotating prism camera, and the resulting images were recorded on 35 mm film (Walker, Scotten & Dewey 1982).

The photographs obtained in this way, such as that in figure 2, showed both the schlieren images of the shock fronts and the grid of laminar smoke jets injected through the holes in the front-surface mirror. The mean particle size in the smoke was submicron and previous work has shown that such smoke acts as an excellent flow tracer in weak shock flows, even within very short distances behind a shock front (Dewey 1964, 1971; Dewey & Whitten 1975; Dewey & Walker 1975). The regularly spaced holes through the mirror could also be seen in the photographs and these served as an array of fiducial markers throughout the field of view.

2.2. *Correction for optical distortion*

The amount of distortion in the photographic images of the shocks and particle tracers was measured. This distortion was caused in part by the off-axis configuration of the schlieren system (approximately 6°), imperfect optical components and the non-uniform shrinkage of photographic paper. To measure and correct for distortion, the positions of the smoke injection holes were accurately measured in the object plane and were compared with the hole positions measured in the photographs. The maximum displacement between points in the matched image and object planes, at the edges of the field of view, was 2.3 mm. The average of the displacement vector magnitudes throughout the field of view was 1.3 mm.

A distortion correction was applied to all measurements made from the photographs, which involved the interpolation of a specific correction factor at each point. The correction factors were interpolated by fitting a plane surface to the observed differences between the actual and measured positions of all the holes in the mirror within a 20 mm radius centred on the point for which the correction factor was being determined. The magnitude of the average error in position in the object plane, after correction, was estimated to be 0.25 mm for a point more than 20 mm from the edge of the field of view, and no more than twice that for a point within 20 mm of the edge of the field of view.

2.3. *Measurement procedures*

Each original photograph on 35 mm film was enlarged approximately 10 times and measurements of shock front and particle tracer positions were made using an x, y digitizer. The measurements were made relative to fiducial markers on the front-surface mirror, and these were in turn related to the leading edge of the wedge. The x and y coordinates were measured at a series of positions along each primary, reflected and Mach stem shock. The coordinates of each particle tracer were also recorded. All measurements were corrected for distortion as described above.

3. Experimental results

3.1. *Shock tube conditions*

Three series of four experiments each were carried out using identical shock tube diaphragm overpressures in each series. The experiments in each series were grouped as close together in time as possible, in order to keep the ambient conditions as unchanged as possible. The mean values of the ambient conditions for each series are shown in table 1. For the subsequent analysis, the results from each experiment were adjusted to standard atmospheric conditions using the measured ambient atmospheric pressure and a computed ambient sound speed. Position coordinates measured in the plane of the front-surface mirror were adjusted by the scale factor $S = P/P_s$, where P and P_s are the measured and standard pressures, respectively, and time values were adjusted by the scale factor Sc/c_s, where c and c_s are the computed and standard sound speeds. Only after these adjustments for the small variations in ambient conditions had been made were the results from the four experiments in each of the three series combined.

The ambient sound speed c used to adjust the experimental results was computed using the measured values of atmospheric pressure P, temperature T and relative humidity as follows:

$$c = 331.45\left[\frac{T+273.16}{273.16}\right]^{\frac{1}{2}}\left[1-\frac{P_w}{P}\left(\frac{\gamma_w}{\gamma}-\frac{5}{8}\right)\right]^{-\frac{1}{2}}, \quad (1)$$

Series number	Atmospheric pressure (kPa)	Ambient temperature (°C)	Relative humidity (%)
1	100.87±0.01	24.7±0.2	46.9±0.4
2	100.99±0.03	24.7±0.0	47.6±0.6
3	100.32±0.02	24.8±0.1	38.6±0.6

TABLE 1. Ambient conditions

where P_w is the pressure of the water vapour in the air. The specific heat ratios for water and air, γ_w and γ, were taken as 1.334 and 1.401, respectively. T is in degrees Celsius.

The standard atmosphere to which results were adjusted was dry air at temperature $T_s = 15$ °C and pressure $P_s = 101325.00$ Pa. The standard atmosphere was considered to be an ideal gas with density $D_s = 1.2250140$ kg m^{-3}, specific heat ratio $\gamma_s = 1.400$ and sound speed $c_s = 340.29205$ m s^{-1}. This is the standard atmosphere of the International Civil Aviation Organization (ICAO). The sound speed in real air at the ICAO standard temperature and pressure is a slightly larger number than c_s above, namely 340.42882 m s^{-1} if (1) is used. An ideal standard gas was chosen, however, so that the experimental results could be used in the analysis which will be presented in Part 2 of this paper, an analysis using ideal-gas equations.

3.2. *Incident shock fronts*

The x and y coordinates of several points along the length of the schlieren image of the incident shock front were measured on each of 74 photographs from the 16 experiments. After correction for optical distortions, the distances between the measured points on a shock front and the straight line joining the end points on the front were computed and the greatest such distance was taken as a measure of the shock front bulge, positive if in the direction of the flow and negative if in the reverse direction. The mean computed bulge was −0.09 mm with a standard deviation of 0.21 mm. This result is comparable both to the thickness of the schlieren image of the shock front, 0.33 mm, and to the estimated error in any measured coordinate value after correction for optical distortion, 0.25 mm. Without the distortion correction, however, the computed mean was 0.28±0.30 mm. The angles between the incident shock fronts and the y axis, defined as perpendicular to the shock tube, were then computed by least-squares fitting straight lines to the shock front data. The mean computed angle was 0.01±0.19°.

Having established that the incident shock fronts were both planar and normal to the x axis, a position coordinate was computed for each shock front which was the average value of the x coordinates for each frame. Incident shock front positions are plotted versus time in figure 3. The trajectories were linear, ±0.24 mm, for each of the three experimental series, and the computed shock velocities are given in table 2. The range of the measured Mach number for the incident shocks in any series of four experiments was less than ±0.4 %.

3.3. *The reflecting surface*

Like the incident shock fronts, the reflecting surface of the wedge appeared in the photographs as a nearly straight line, and values of bulge were computed using points measured on these lines and corrected for optical distortion. A small concave bulge

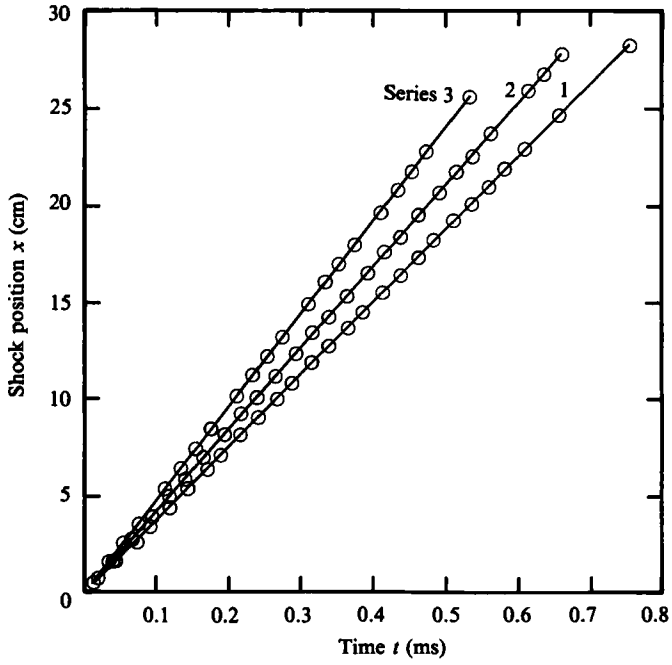

FIGURE 3. Trajectories of the incident shock fronts in the three experimental series. The points are measured data and the lines are least-squares fits to the data. The origin is defined to be such that the shock is at the upstream edge of the mirror at time $t = 0$. The wedge tip is at $x = 4$ cm.

Series number	Incident shock speed (Mach no.)	Reflected shock speed (local Mach no.)	Centre point speed (Mach no.)	Computed peak incident flow speed (Mach no.)	Measured average incident flow speed (Mach no.)	Triple-point trajectory angle (degrees)	Incident-reflected shock front angle (degrees)
1	1.105 ±0.001	1.001 ±0.005	0.179 ±0.002	0.166 ±0.002	0.161 ±0.007	21.95 ±0.13	25.19 ±1.44
2	1.240 ±0.002	1.013 ±0.006	0.360 ±0.003	0.362 ±0.002	0.351 ±0.012	27.00 ±0.09	35.30 ±0.57
3	1.415 ±0.002	1.012 ±0.013	0.596 ±0.003	0.590 ±0.002	0.582 ±0.016	28.98 ±0.11	42.99 ±1.50

TABLE 2. Measured incident and reflected shock front data

or 'sag' in the reflecting surface was computed, of 0.60 ± 0.45 mm or approximately 0.3% of the total length of the surface. This value exceeded that measured directly in the laboratory, a value less than 0.05 mm or 0.02% of the total length, and the difference was attributed to the fact that the wedge surface was a boundary of the region in which the distortion correction data were measured. The effect of the difference on other measurements was considered to be negligible.

The angle between the reflecting surface and the x-axis, and the intercept with the x axis, where the x axis was defined to lie on the shock tube floor, were computed from the photographic data by fitting least-squares straight lines to the points

measured on the wedge surface. The mean computed angle was $10.01 \pm 0.17°$ and the mean computed intercept was 3.99 ± 0.39 cm. Both computed values agreed with the values measured directly in the laboratory, namely $10.04 \pm 0.03°$ and 4.00 ± 0.05 cm, respectively.

3.4. *Triple-point trajectories*

The coordinates of the triple point, the junction of the incident, reflected and Mach stem shock fronts, were measured in each photograph. For each experimental series the triple-point trajectories were straight. The mean computed bulge values were at -0.79 ± 1.37, -0.40 ± 0.46 and 0.23 ± 0.62 mm, for series 1, 2 and 3, respectively, the negative values representing sag. The mean of these values is -0.32 ± 0.93 mm, about 1.25 % of the observed length of the trajectory. The triple-point data were then least-squares fitted with straight lines and the results are plotted in figure 4. The angles between the trajectories and the horizontal are included in table 2.

The intercepts with the x axis of the triple-point trajectories shown in figure 4 were computed at 3.92 ± 0.40, 4.04 ± 0.26 and 4.02 ± 0.31 cm (mean value 3.99 ± 0.30 cm). When compared with the values of the x coordinate of the wedge tip measured in the laboratory and photographically, respectively of 4.00 ± 0.05 cm and 3.99 ± 0.39 cm, and using a t-test, no significant difference between the triple-point intercept and the wedge tip position could be detected in any of the three series.

3.5. *Reflected shocks*

From each schlieren photograph the x and y coordinates of approximately 15 points on the reflected shock were measured. Circles were fitted by the method of least squares to these data and the centres of the circles determined. The results for five of the pictures from one experiment are shown as figure 5. In each photograph, and for all experiments, the reflected shocks appeared to be perfectly circular. The mean standard deviation for the 64 circle fits was ± 0.15 mm, less than that for the straight line incident shock front fits and less than the average thickness of the schlieren images of the shock fronts. Careful inspection of the photographs revealed no small deviations from circularity near the triple point.

Figures 6 and 7 show respectively the radii of the reflected shocks and the x coordinates of the centres of the fitted circles, plotted versus time. The Mach numbers of these shocks are given in table 2. The reflected shocks were weak in all cases, with velocities only slightly greater than the sound speeds computed behind the incident shocks. The centres of the circles fitted to the reflected shock lay on the floor of the shock tube and moved with the velocity of the gas flow behind the primary shock. The velocities of the centres are compared in table 2 with the particle velocities behind the incident shocks as computed from the incident shock speed and as measured from the particle tracers, averaged over the entire incident flow field.

The angle between the reflected and the incident shocks at the triple point was computed for each of the 64 photographs, using the measured values of the triple-point position and the radius and the centre position of the reflected shock. The results are included in table 2.

3.6. *Mach stem shocks*

The Mach stem shocks in all these experiments were curved. The coordinates of approximately 15 points on each Mach stem shock were measured and fitted to a second-order polynomial. No improvement to the fit was obtained by using a higher order. In order to measure the normal velocity of the Mach stem shock at any point along its length, a family of curves orthogonal to the Mach stem shocks were also

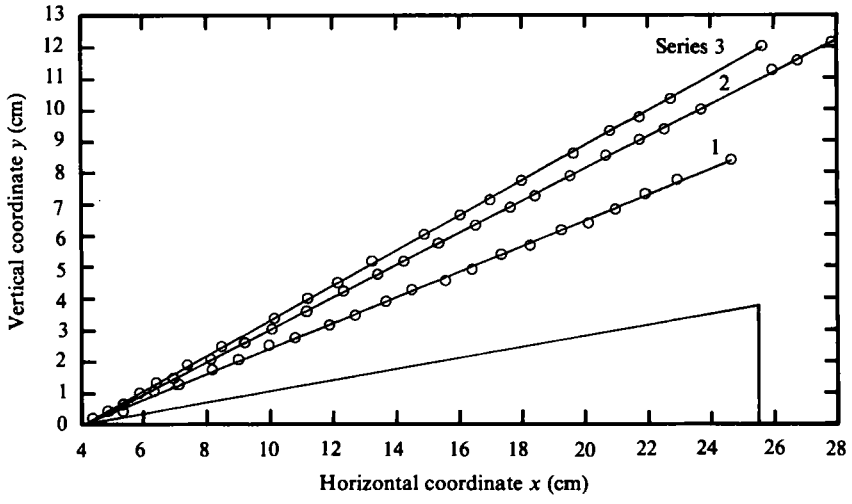

FIGURE 4. Trajectory of the triple point in each of the experimental series. Points are measured data and the lines are least-squares fits.

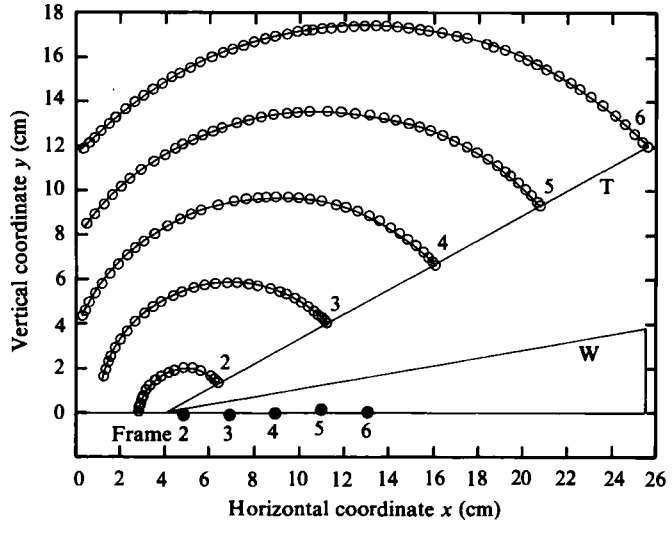

FIGURE 5. Shape of the reflected shock front at five times in the second experiment of series 3. W indicates the wedge surface and T, the triple-point trajectory. ○ represent measured data; the curves are least-squares fits to those data; ● represent the shock centre points, computed in the fitting process.

fitted. Figure 8 shows the Mach stem shocks and orthogonal rays fitted to the results of one of the experimental series.

The displacement of the Mach stem shock along an orthogonal was measured, and found to be linear with time along all orthogonals in each experiment. The data for the lowest orthogonal in each experimental series are shown in figure 9. Mach stem shock speed, i.e. the slope of the displacement-time fit, is plotted as a function of height above the wedge surface in figure 10. The accuracy with which it was possible to determine the speed decreased with height, because as the triple point was approached the shock trajectory along an orthogonal was determined at fewer points.

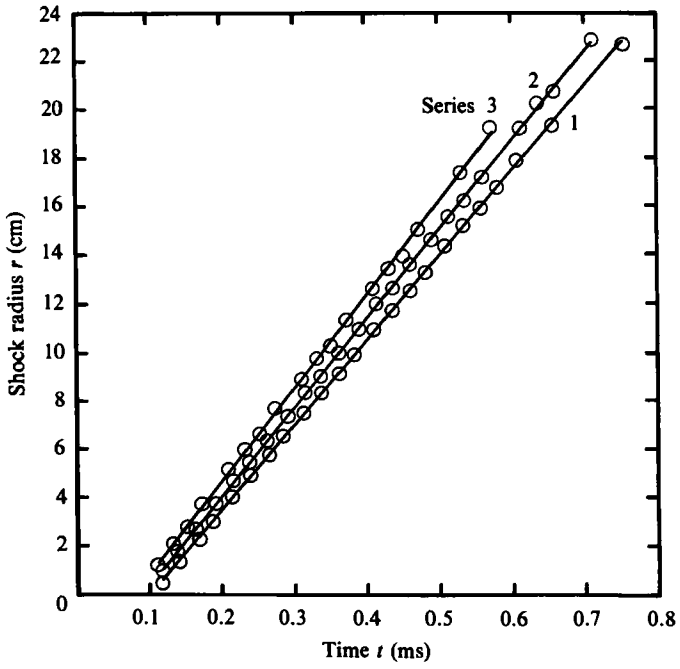

FIGURE 6. Trajectories of the reflected shock fronts for the three experimental series. The points represent measured data and the lines, least-squares fits to those data. The time origin is as for figure 3.

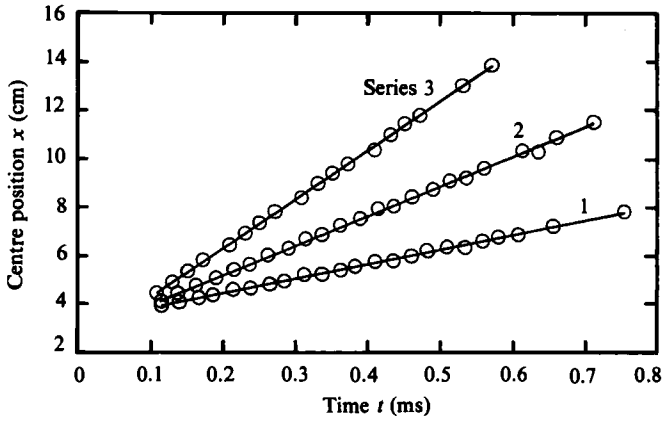

FIGURE 7. Trajectories of the centres of the circular reflected shock fronts in the three experimental series. The points represent measured data and the lines, least-squares fits to those data. The time origin is as for figure 3.

In each experimental series, there was a gradual decrease in the Mach stem shock velocity as the triple point was approached. Within the limits of experimental accuracy this decrease appeared to be linear, as indicated by the dashed lines in figure 10.

The curves orthogonal to the Mach stem shocks could be started at any point on any shock. For an initial point chosen at the foot of a Mach stem, that is, on the surface of the wedge, it was expected that the orthogonal would remain a straight line on the surface of the wedge. This was not the case (see figure 8), implying that

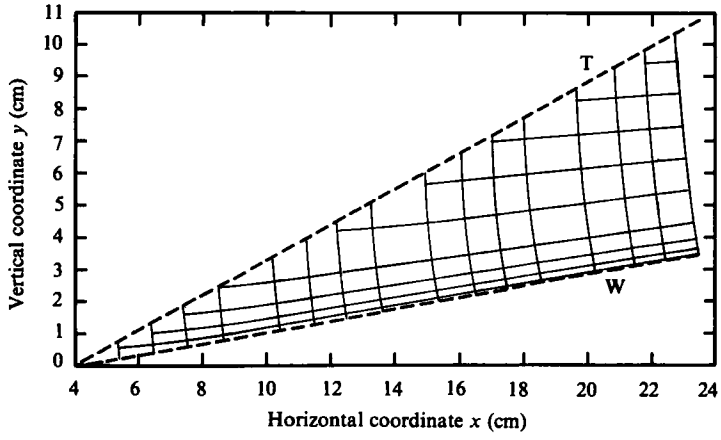

FIGURE 8. Illustration of Mach stem shock analysis in the third experimental series. The dashed lines approximate the wedge surface and the triple-point trajectory. The vertical solid curves are polynomial fits to Mach stem shock data and the horizontal solid curves are orthogonal rays, which were propagated from the shock front on the right-hand side.

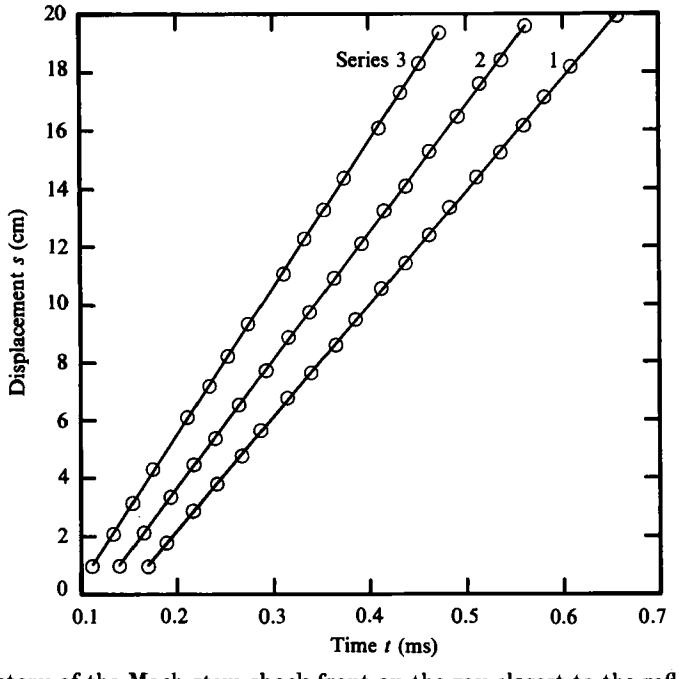

FIGURE 9. Trajectory of the Mach stem shock front on the ray closest to the reflecting surface in each experimental series. Points are measured data and the lines are least-squares fits. Displacement is arbitrarily set at 1 cm for the first point. The time origin is as for figure 3.

the Mach stem shocks were not exactly perpendicular to the surface of the wedge. A careful study of the schlieren photographs from these and other experiments with incident shock strengths in the range discussed here, suggests that the Mach stem shock is not always perpendicular to the reflecting surface, but may be inclined forward a small amount, as much as 1°.

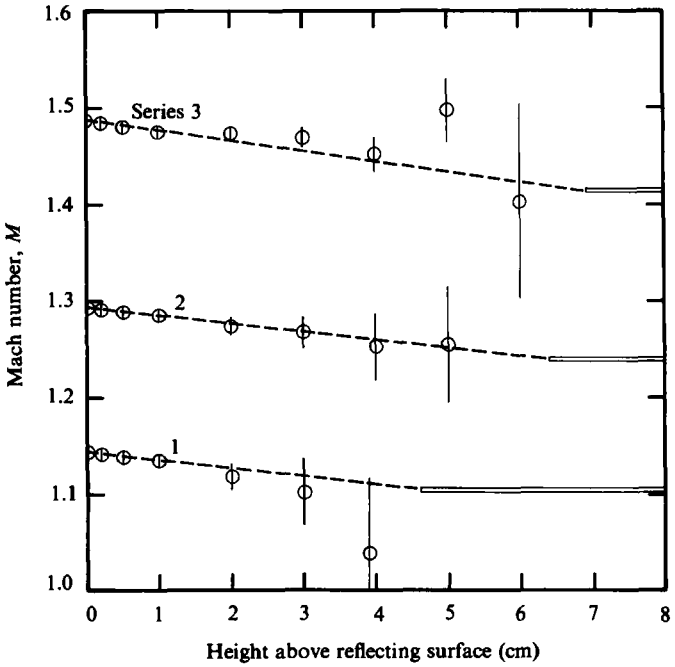

FIGURE 10. Variation of Mach stem shock strength with distance from the reflecting surface, for each experimental series. The points each represent data for one orthogonal ray with error bars increasing in size as the ray length decreases. Height is measured vertically up the longest shock front, the one nearest the end of the wedge. The incident shock strength and its uncertainty are shown for each experimental series as a double horizontal line.

The angles between the tangent to the Mach stem shock and the incident shock at the triple point, and between the tangent to the Mach stem shock at the wedge surface and the normal to the wedge surface, were measured for each schlieren photograph. At the triple point the computed angles were respectively 0.0 ± 0.6, 1.2 ± 0.3 and $2.3 \pm 0.5°$ for series 1, 2 and 3. At the wedge surface the corresponding mean angles were 0.0 ± 0.08, 1.0 ± 0.4 and $1.0 \pm 1.1°$ forward from the perpendicular to the wedge surface.

The shape of the Mach stem shocks was also studied by fitting the points measured along the shocks with circles instead of polynomial functions. For each of the experimental series the centres of the best circle fits defined a straight line parallel to and slightly below the reflecting surface, about 5 mm below the surface in series 1 and about 10 mm in series 2 and 3. The shock angles at both the triple point and the wedge surface were similar to those obtained using polynomial fits, and also indicated a small forward inclination of the Mach stem at the wedge surface.

3.7. *Measurement of the particle trajectories*

For each smoke particle tracer, plots were made of the x coordinate versus time and the y coordinate versus time, where the x and y axes were defined as being parallel to the shock tube floor and to the incident shock, respectively. Tracer positions were corrected for optical distortion. The time at which a shock front arrived at a tracer was identified as a discontinuity in the derivative of the particle trajectory.

The coordinates of each tracer before the arrival of the first shock were averaged to determine the initial tracer position (x_0, y_0). The x, t and y, t trajectories of each

tracer between shock arrivals were then described by least-squares fits to polynomial functions, using the lowest order which appeared to describe adequately the trajectory. In this series of experiments most of the data could be described adequately using polynomials of the first order. These polynomials were then used to interpolate the x, y coordinates of the tracers at intermediate times. The slopes of the polynomials at these times were calculated to provide the velocity components $\mathrm{d}x/\mathrm{d}t$ and $\mathrm{d}y/\mathrm{d}t$.

The Lagrangian form of the equation of continuity in two dimensions may be written as

$$\frac{\rho_0}{\rho} = \begin{bmatrix} \dfrac{\partial x}{\partial x_0} & \dfrac{\partial y}{\partial x_0} \\ \dfrac{\partial x}{\partial y_0} & \dfrac{\partial y}{\partial y_0} \end{bmatrix},$$

where ρ_0 and ρ are the ambient density of the gas before the arrival of the first shock, and the density at any subsequent time, respectively. Alternatively this equation may be written $\rho_0/\rho = A/A_0$, where A and A_0 are the areas of elemental cells defined by three or four adjacent tracers in the object plane, respectively before and after passage of the initial shock front. The gas density calculated in this way was thus the average value over a volume for which the elemental cell was a uniform cross-section. This value of the density was assigned to the centroid of the cell.

As each elemental cell was traversed by a shock, the pressure ratio P_1/P_0 and the density ratio ρ_1/ρ_0 were computed from the shock Mach number using the normal shock relations, where P_1 and ρ_1 are the values of pressure and density immediately behind the shock, and P_0 and ρ_0 are the ambient values ahead of the shock. Assuming that the flow of each air element was isentropic between shock fronts, the hydrostatic pressure P at a time after the first shock arrival was computed using

$$\frac{P}{P_0} = \frac{P_1}{P_0}\left[\frac{\rho}{\rho_0}\right]^\gamma \left[\frac{\rho_0}{\rho_1}\right]^\gamma = \frac{P_1}{P_0}\left[\frac{\rho}{\rho_1}\right]^\gamma,$$

where γ is the ratio of specific heats for air. This relationship was used only in a Lagrangian coordinate system because some of the shock waves considered may have been unsteady and if so would have left the gas in a state of spatially varying entropy. If a gas element was traversed by the reflected shock, the normal shock relations were used again to compute the second entropy change, that is, to compute new values of the pressure and density ratios, respectively P_2/P_1 and ρ_2/ρ_1.

From the analysis of the particle trajectories, mappings of the particle velocity, density and pressure were obtained throughout the flow field at a series of times for each series of experiments. A typical array of particle velocity vectors is shown in figure 11. Simple vector transformations can be made to such a flow field to show the velocity vectors relative to points in the flow-field. For example, figure 12 shows the velocity vectors behind the reflected and Mach stem shocks relative to the mean particle velocity behind the primary shock.

The particle velocities behind the incident shock fronts were constant over the region in front of the reflected shocks, within the estimated uncertainties of measurement. The average velocity in this region for each series is included in table 2, compared to the value computed using the incident shock Mach number and the Rankine–Hugoniot equations.

The average measured density, hydrostatic overpressure and dynamic pressure for

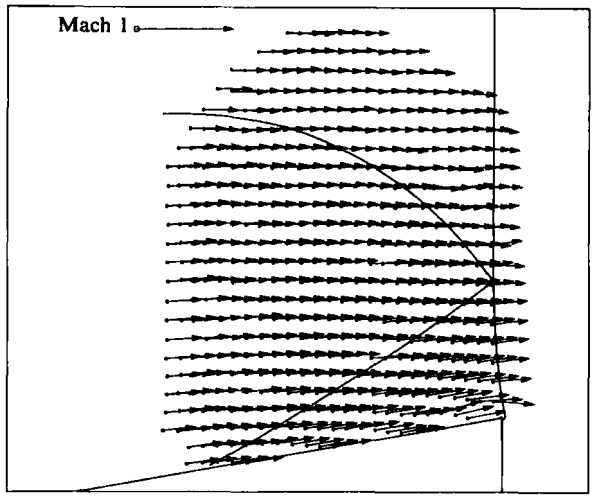

FIGURE 11. Particle velocity vectors from experimental series 2, at the time when the shock system is just over the wedge. The contact surface could not be seen in the schlieren photographs in this series and its position was inferred from the particle trajectories.

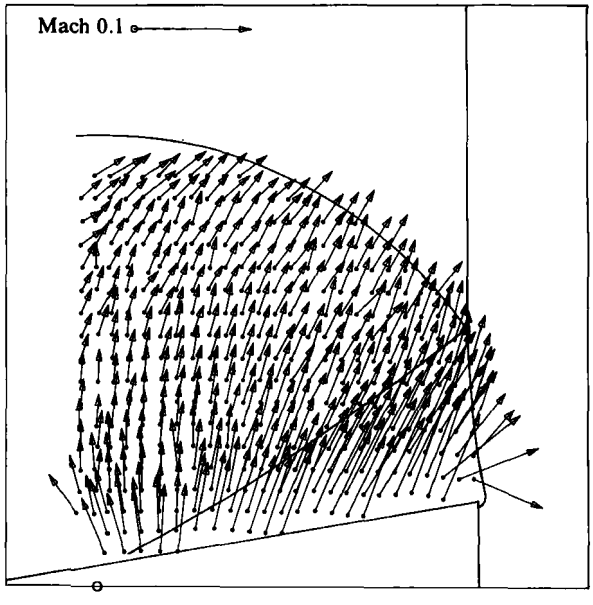

FIGURE 12. A transformation of the flow shown in figure 11. The average velocity in the region behind the incident shock has been subtracted from all vectors in figure 11, in order to show the relative flow pattern. Also shown above are the slipstream and the reflected shock centre point.

each of the regions behind the incident, reflected and Mach stem shocks are given in table 3, compared to the computed peak, Rankine–Hugoniot values. All values are normalized to ambient density and pressure. In the Mach stem region consideration was restricted to those cells nearest the wedge surface, and the Mach number which was measured on the lowest orthogonal ray was the one used in the Rankine–Hugoniot equations. In all cases, cells intersected by shock fronts were excluded from the average.

Series number	Region	Density ratio		Hydrostatic overpressure ratio		Dynamic pressure ratio	
		Peak computed	Average measured	Peak computed	Average measured	Peak computed	Average measured
1	Incident	1.177±0.002	1.183±0.018	0.257±0.003	0.265±0.027	0.023±0.001	0.021±0.004
	Reflected	1.179±0.011	1.198±0.052	0.259±0.014	0.289±0.079	†	0.025±0.008
	Mach stem at wedge	1.245±0.005	1.217±0.121	0.361±0.008	0.322±0.186	0.044±0.002	0.029±0.020
2	Incident	1.412±0.003	1.411±0.031	0.629±0.005	0.627±0.051	0.129±0.002	0.122±0.014
	Reflected	1.443±0.016	1.450±0.060	0.660±0.018	0.691±0.098	†	0.143±0.024
	Mach stem at wedge	1.503±0.006	1.480±0.039	0.784±0.010	0.745±0.065	0.197±0.005	0.162±0.021
3	Incident	1.715±0.003	1.723±0.053	1.168±0.005	1.183±0.094	0.418±0.004	0.409±0.034
	Reflected	1.749±0.040	1.802±0.098	1.197±0.036	1.325±0.176	†	0.471±0.055
	Mach stem at wedge	1.840±0.005	1.874±0.062	1.413±0.011	1.477±0.115	0.593±0.008	0.551±0.041

† Peak dynamic pressure varies along the reflected shock front, measured in laboratory frame of reference

TABLE 3. Average measured densities and pressures (incident shock at $x = 20$ cm)

3.8. *The contact surface*

Henderson (1983) has proposed a model to describe Mach reflection in terms of the angles at the triple point between the three shocks and the contact surface which separates the gas behind the reflected shock from the gas behind the Mach stem shock. The angles measured between the incident and reflected shocks at the triple point in the three experiments described here are given in table 2, and the corresponding angles for the Mach stem have been given above. The contact surface was identified in the schlieren photographs of series 3 (incident shock Mach number 1.415), but it could not be detected in the photographs of series 1 and 2 (Mach numbers 1.105 and 1.240), even with optimum sensitivity of the schlieren system. This is not surprising since the ratios of the densities across the contact surfaces in series 1 and 2 were calculated to be respectively 1.00005 and 1.00037. The ratio is series 3, in which the contact surface was detected, was 1.00140.

An attempt was made to measure the slope of the contact surfaces using the velocity vectors of the particle flow tracers between which the triple point had passed. These velocity vectors were adjusted relative to the triple-point velocity vector. The results are plotted in figure 13. For each shock strength the plotted angle appears to be converging to a constant value, because the relative distance between the point of measurement and the triple point decreases as the configuration of the shocks grows with time. The apparent time dependency arises from the spatial resolution of the measurement, and does not indicate a lack of self-similarity. The spatial resolution of this technique is limited by the 1 cm spacing of the flow tracers.

For series 3, in which the contact surface could be identified in the schlieren photographs, the observed slopes of the contact surface at the triple point, and 1.5 cm behind the triple point, are also plotted. The measurements made behind the triple point are similar to those made using the flow tracer velocity vectors, and show the same apparent time dependency.

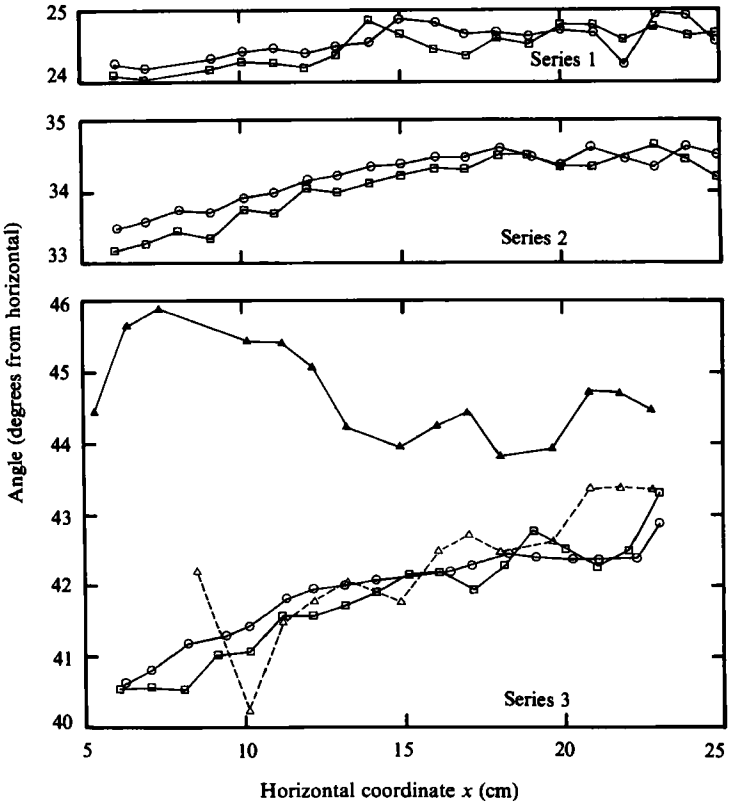

FIGURE 13. Particle velocity vector angle near the triple point versus the triple-point position for each experimental series. ○ and □ represent data measured just above and below the contact surface, respectively. ▲ and △ represent data measured from schlieren images of the contact surface in series 3, at the triple point (——) and 1.5 cm behind the triple point (– – – –).

4. Discussion and conclusions

The purpose of the experiments described here was to determine as accurately as possible the position and shapes of the shocks and the flow-fields associated with the Mach reflection of a weak plane shock. This goal has been largely achieved. The array of holes in the front-surface mirror provided a grid of fiducial markers which has permitted an accurate determination of the positions of shocks and the smoke tracers throughout the field of view. As a result, the measurements presented above provide a consistent picture of the phenomenon of Mach reflection and permit a number of conclusions to be drawn. In the analysis of the Mach reflection of non-stationary shocks it is normally assumed that the flow is self-similar, so that if the flow-field is scaled linearly with respect to a displacement, such as the distance of the foot of the Mach stem from the leading edge of the wedge, the flows will appear independent of time. The self-similarity of the flow in each of the three series described here was evaluated by linear scaling of the positions of the shocks and of the particle velocity vectors at three times. This evaluation indicated no departure from self-similarity of the flow-fields, and the assumption of self-similarity for the Mach reflection of weak plane shocks would appear to be justified.

At this time, the structure of the flow throughout the three regions behind the incident, reflected and Mach stem shocks has not been studied in detail. Behind the

incident shock there appears to be a random variation of the flow-field. The average values of the particle velocity calculated from the particle tracer positions in three experiments were very near to the peak values calculated from the observed shock velocity. Some structure may be found in the flow-field behind the reflected shock front and in that behind the Mach stem shock, but the limited number of particle tracers in these regions does not permit an accurate description.

For the incident shock strengths and reflection angle considered here, the cross-sections of the reflected shocks were circular with the centres of the circles moving at the velocity of the flow behind the incident shock, and, within the limits of experimental accuracy, no variation in the velocity of the reflected shock could be observed.

The Mach stem shocks in all of the experiments discussed here were curved and their cross-sections were well described by circles centred on a point slightly below the reflecting surface. Careful inspection of high-resolution schlieren photographs of the foot of the Mach stem indicated that the Mach stem shocks in these experiments were not exactly perpendicular to the wedge surface but had a slight forward inclination of as much as 1°. The speed of the Mach stem shock appeared to be constant along any one orthogonal ray and to decrease monotonically with height above the reflecting surface.

In all the experiments, the trajectory of the triple point was linear, and the angle between this trajectory and the surface of the wedge was found, where a comparison was possible, to agree well with the values reported by Henderson & Siegenthaler (1980). In Part 2 of this paper it will be pointed out that, to model Mach reflection, knowledge of at least one parameter determined from experimental measurements is required. The inclination of the triple-point trajectory as a function of the incident shock strength and wedge angle may be the most convenient parameter to use for this purpose.

The availability of the time-resolved particle trajectories makes it possible to apply oblique shock theory to the phenomenon of Mach reflection, and this is presented in Part 2 of this paper.

The authors gratefully acknowledge the assistance of L. N. Scotten and A. W. Y. Chan who carried out the experiments described here. Financial support of this work was provided by the Defence Research Establishment Suffield; the Natural Sciences and Engineering Research Council of Canada; the Scientific Affairs Division of NATO, and the University of Victoria.

REFERENCES

Ben-Dor, G. 1980 *Can. Aero. & Space J.* **26**, 98.

Ben-Dor, G. & Glass, I. I. 1978 *AIAA J.* **16**, 1146.

Ben-Dor, G. & Glass, I. I. 1979 *J. Fluid Mech.* **92**, 459.

Ben-Dor, G. & Glass, I. I. 1980 *J. Fluid Mech.* **96**, 735.

Ben-Dor, G., Whitten, B. T. & Glass, I. I. 1979 *Intl J. Heat and Fluid Flow* **1**, 77.

Boys, C. V. 1893 *Nature* **47**, 440.

Dewey, J. M. 1964 *Proc. R. Soc. Lond.* A **279**, 366.

Dewey, J. M. 1971 *Proc. R. Soc. Lond.* A **324**, 275.

Dewey, J. M., Heilig, W., Reichenbach, H. & Walker, D. K. 1983 In *Proc. 3rd Intl Symp. Flow Visualization*, p. 585.

Dewey, J. M. & McMillin, D. J. 1981 *Can. J. Phys.* **59**, 1380.

DEWEY, J. M., MCMILLIN, D. J. & CLASSEN, D. F. 1977 *J. Fluid Mech.* **81**, 701.

DEWEY, J. M. & MCMILLIN, D. J. 1985 *J. Fluid Mech.* **152**, 67–81.

DEWEY, J. M. & WALKER, D. K. 1975 *J. Appl. Phys.* **46**, 3454.

DEWEY, J. M. & WHITTEN, B. T. 1975 *Phys. Fluids* **18**, 437.

HENDERSON, L. F. 1983 In *Proc. 14th Sym. Shock Tube & Waves*, p. 144.

HENDERSON, L. F. & LOZZI, A. 1979 *J. Fluid Mech.* **94**, 541.

HENDERSON, L. F. & SIEGENTHALER, A. 1980 *Proc. R. Soc. Lond.* A **369**, 537.

INTERNATIONAL CIVIL AVIATION ORGANIZATION STANDARD ATMOSPHERE (U.S. EXTENSION TO) 1958 As quoted in *Handbook of Chemistry and Physics 56th ed.*, F-201. CRC Press, Cleveland.

JONES, D. M., MARTIN, P. M. E. & THORNHILL, G. K. 1951 *Proc. R. Soc. Lond.* A **209**, 238.

MACH, E. 1878 *Akad. Wiss. Wien* **77**, 1228.

WALKER, D. K., SCOTTEN, L. N. & DEWEY, J. M. 1982 In *Proc. 15th Intl Cong. High Speed Photo. and Photonics*, *SPIE* **348**, 125.